FERMILAB-PUB-12-403-E

Search for the standard model Higgs boson in $ZH \to \ell^+\ell^- b\bar{b}$ production with the D0 detector in 9.7 fb^{-1} of $p\bar{p}$ collisions at $\sqrt{s} = 1.96$ TeV

V.M. Abazov,[32] B. Abbott,[69] B.S. Acharya,[26] M. Adams,[46] T. Adams,[44] G.D. Alexeev,[32] G. Alkhazov,[36] A. Alton[a],[58] G. Alverson,[57] A. Askew,[44] S. Atkins,[55] K. Augsten,[7] C. Avila,[5] F. Badaud,[10] L. Bagby,[45] B. Baldin,[45] D.V. Bandurin,[44] S. Banerjee,[26] E. Barberis,[57] P. Baringer,[53] J.F. Bartlett,[45] U. Bassler,[15] V. Bazterra,[46] A. Bean,[53] M. Begalli,[2] L. Bellantoni,[45] S.B. Beri,[24] G. Bernardi,[14] R. Bernhard,[19] I. Bertram,[39] M. Besançon,[15] R. Beuselinck,[40] P.C. Bhat,[45] S. Bhatia,[60] V. Bhatnagar,[24] G. Blazey,[47] S. Blessing,[44] K. Bloom,[61] A. Boehnlein,[45] D. Boline,[66] E.E. Boos,[34] G. Borissov,[39] T. Bose,[56] A. Brandt,[72] O. Brandt,[20] R. Brock,[59] A. Bross,[45] D. Brown,[14] J. Brown,[14] X.B. Bu,[45] M. Buehler,[45] V. Buescher,[21] V. Bunichev,[34] S. Burdin[b],[39] C.P. Buszello,[38] E. Camacho-Pérez,[29] B.C.K. Casey,[45] H. Castilla-Valdez,[29] S. Caughron,[59] S. Chakrabarti,[66] D. Chakraborty,[47] K.M. Chan,[51] A. Chandra,[74] E. Chapon,[15] G. Chen,[53] S. Chevalier-Théry,[15] D.K. Cho,[71] S.W. Cho,[28] S. Choi,[28] B. Choudhary,[25] S. Cihangir,[45] D. Claes,[61] J. Clutter,[53] M. Cooke,[45] W.E. Cooper,[45] M. Corcoran,[74] F. Couderc,[15] M.-C. Cousinou,[12] A. Croc,[15] D. Cutts,[71] A. Das,[42] G. Davies,[40] S.J. de Jong,[30,31] E. De La Cruz-Burelo,[29] F. Déliot,[15] R. Demina,[65] D. Denisov,[45] S.P. Denisov,[35] S. Desai,[45] C. Deterre,[15] K. DeVaughan,[61] H.T. Diehl,[45] M. Diesburg,[45] P.F. Ding,[41] A. Dominguez,[61] A. Dubey,[25] L.V. Dudko,[34] D. Duggan,[62] A. Duperrin,[12] S. Dutt,[24] A. Dyshkant,[47] M. Eads,[61] D. Edmunds,[59] J. Ellison,[43] V.D. Elvira,[45] Y. Enari,[14] H. Evans,[49] A. Evdokimov,[67] V.N. Evdokimov,[35] G. Facini,[57] L. Feng,[47] T. Ferbel,[65] F. Fiedler,[21] F. Filthaut,[30,31] W. Fisher,[59] H.E. Fisk,[45] M. Fortner,[47] H. Fox,[39] S. Fuess,[45] A. Garcia-Bellido,[65] J.A. García-González,[29] G.A. García-Guerra[c],[29] V. Gavrilov,[33] P. Gay,[10] W. Geng,[12,59] D. Gerbaudo,[63] C.E. Gerber,[46] Y. Gershtein,[62] G. Ginther,[45,65] G. Golovanov,[32] A. Goussiou,[76] P.D. Grannis,[66] S. Greder,[16] H. Greenlee,[45] G. Grenier,[17] Ph. Gris,[10] J.-F. Grivaz,[13] A. Grohsjean[d],[15] S. Grünendahl,[45] M.W. Grünewald,[27] T. Guillemin,[13] G. Gutierrez,[45] P. Gutierrez,[69] S. Hagopian,[44] J. Haley,[57] L. Han,[4] K. Harder,[41] A. Harel,[65] J.M. Hauptman,[52] J. Hays,[40] T. Head,[41] T. Hebbeker,[18] D. Hedin,[47] H. Hegab,[70] A.P. Heinson,[43] U. Heintz,[71] C. Hensel,[20] I. Heredia-De La Cruz,[29] K. Herner,[58] G. Hesketh[f],[41] M.D. Hildreth,[51] R. Hirosky,[75] T. Hoang,[44] J.D. Hobbs,[66] B. Hoeneisen,[9] J. Hogan,[74] M. Hohlfeld,[21] I. Howley,[72] Z. Hubacek,[7,15] V. Hynek,[7] I. Iashvili,[64] Y. Ilchenko,[73] R. Illingworth,[45] A.S. Ito,[45] S. Jabeen,[71] M. Jaffré,[13] A. Jayasinghe,[69] M.S. Jeong,[28] R. Jesik,[40] P. Jiang,[4] K. Johns,[42] E. Johnson,[59] M. Johnson,[45] A. Jonckheere,[45] P. Jonsson,[40] J. Joshi,[43] A.W. Jung,[45] A. Juste,[37] K. Kaadze,[54] E. Kajfasz,[12] D. Karmanov,[34] P.A. Kasper,[45] I. Katsanos,[61] R. Kehoe,[73] S. Kermiche,[12] N. Khalatyan,[45] A. Khanov,[70] A. Kharchilava,[64] Y.N. Kharzheev,[32] I. Kiselevich,[33] J.M. Kohli,[24] A.V. Kozelov,[35] J. Kraus,[60] S. Kulikov,[35] A. Kumar,[64] A. Kupco,[8] T. Kurča,[17] V.A. Kuzmin,[34] S. Lammers,[49] G. Landsberg,[71] P. Lebrun,[17] H.S. Lee,[28] S.W. Lee,[52] W.M. Lee,[45] X. Lei,[42] J. Lellouch,[14] D. Li,[14] H. Li,[11] L. Li,[43] Q.Z. Li,[45] J.K. Lim,[28] D. Lincoln,[45] J. Linnemann,[59] V.V. Lipaev,[35] R. Lipton,[45] H. Liu,[73] Y. Liu,[4] A. Lobodenko,[36] M. Lokajicek,[8] R. Lopes de Sa,[66] H.J. Lubatti,[76] R. Luna-Garcia[g],[29] A.L. Lyon,[45] A.K.A. Maciel,[1] R. Madar,[15] R. Magaña-Villalba,[29] S. Malik,[61] V.L. Malyshev,[32] Y. Maravin,[54] J. Martínez-Ortega,[29] R. McCarthy,[66] C.L. McGivern,[41] M.M. Meijer,[30,31] A. Melnitchouk,[60] D. Menezes,[47] P.G. Mercadante,[3] M. Merkin,[34] A. Meyer,[18] J. Meyer,[20] F. Miconi,[16] N.K. Mondal,[26] M. Mulhearn,[75] E. Nagy,[12] M. Naimuddin,[25] M. Narain,[71] R. Nayyar,[42] H.A. Neal,[58] J.P. Negret,[5] P. Neustroev,[36] H.T. Nguyen,[75] T. Nunnemann,[22] J. Orduna,[74] N. Osman,[12] J. Osta,[51] M. Padilla,[43] A. Pal,[72] N. Parashar,[50] V. Parihar,[71] S.K. Park,[28] R. Partridge[e],[71] N. Parua,[49] A. Patwa,[67] B. Penning,[45] M. Perfilov,[34] Y. Peters,[41] K. Petridis,[41] G. Petrillo,[65] P. Pétroff,[13] M.-A. Pleier,[67] P.L.M. Podesta-Lerma[h],[29] V.M. Podstavkov,[45] A.V. Popov,[35] M. Prewitt,[74] D. Price,[49] N. Prokopenko,[35] J. Qian,[58] A. Quadt,[20] B. Quinn,[60] M.S. Rangel,[1] K. Ranjan,[25] P.N. Ratoff,[39] I. Razumov,[35] P. Renkel,[73] I. Ripp-Baudot,[16] F. Rizatdinova,[70] M. Rominsky,[45] A. Ross,[39] C. Royon,[15] P. Rubinov,[45] R. Ruchti,[51] G. Sajot,[11] P. Salcido,[47] A. Sánchez-Hernández,[29] M.P. Sanders,[22] A.S. Santos[i],[1] G. Savage,[45] L. Sawyer,[55] T. Scanlon,[40] R.D. Schamberger,[66] Y. Scheglov,[36] H. Schellman,[48] S. Schlobohm,[76] C. Schwanenberger,[41] R. Schwienhorst,[59] J. Sekaric,[53] H. Severini,[69] E. Shabalina,[20] V. Shary,[15] S. Shaw,[59] A.A. Shchukin,[35] R.K. Shivpuri,[25] V. Simak,[7] P. Skubic,[69] P. Slattery,[65] D. Smirnov,[51] K.J. Smith,[64] G.R. Snow,[61] J. Snow,[68] S. Snyder,[67] S. Söldner-Rembold,[41] L. Sonnenschein,[18] K. Soustruznik,[6] J. Stark,[11] D.A. Stoyanova,[35] M. Strauss,[69] L. Suter,[41] P. Svoisky,[69] M. Takahashi,[41] M. Titov,[15] V.V. Tokmenin,[32] Y.-T. Tsai,[65] K. Tschann-Grimm,[66] D. Tsybychev,[66] B. Tuchming,[15] C. Tully,[63] L. Uvarov,[36] S. Uvarov,[36] S. Uzunyan,[47] R. Van Kooten,[49] W.M. van Leeuwen,[30] N. Varelas,[46] E.W. Varnes,[42] I.A. Vasilyev,[35] P. Verdier,[17]

A.Y. Verkheev,[32] L.S. Vertogradov,[32] M. Verzocchi,[45] M. Vesterinen,[41] D. Vilanova,[15] P. Vokac,[7] H.D. Wahl,[44] M.H.L.S. Wang,[45] J. Warchol,[51] G. Watts,[76] M. Wayne,[51] J. Weichert,[21] L. Welty-Rieger,[48] A. White,[72] D. Wicke,[23] M.R.J. Williams,[39] G.W. Wilson,[53] M. Wobisch,[55] D.R. Wood,[57] T.R. Wyatt,[41] Y. Xie,[45] R. Yamada,[45] S. Yang,[4] W.-C. Yang,[41] T. Yasuda,[45] Y.A. Yatsunenko,[32] W. Ye,[66] Z. Ye,[45] H. Yin,[45] K. Yip,[67] S.W. Youn,[45] J.M. Yu,[58] J. Zennamo,[64] T. Zhao,[76] T.G. Zhao,[41] B. Zhou,[58] J. Zhu,[58] M. Zielinski,[65] D. Zieminska,[49] and L. Zivkovic[71]

(The D0 Collaboration*)

[1]*LAFEX, Centro Brasileiro de Pesquisas Físicas, Rio de Janeiro, Brazil*
[2]*Universidade do Estado do Rio de Janeiro, Rio de Janeiro, Brazil*
[3]*Universidade Federal do ABC, Santo André, Brazil*
[4]*University of Science and Technology of China, Hefei, People's Republic of China*
[5]*Universidad de los Andes, Bogotá, Colombia*
[6]*Charles University, Faculty of Mathematics and Physics, Center for Particle Physics, Prague, Czech Republic*
[7]*Czech Technical University in Prague, Prague, Czech Republic*
[8]*Center for Particle Physics, Institute of Physics, Academy of Sciences of the Czech Republic, Prague, Czech Republic*
[9]*Universidad San Francisco de Quito, Quito, Ecuador*
[10]*LPC, Université Blaise Pascal, CNRS/IN2P3, Clermont, France*
[11]*LPSC, Université Joseph Fourier Grenoble 1, CNRS/IN2P3, Institut National Polytechnique de Grenoble, Grenoble, France*
[12]*CPPM, Aix-Marseille Université, CNRS/IN2P3, Marseille, France*
[13]*LAL, Université Paris-Sud, CNRS/IN2P3, Orsay, France*
[14]*LPNHE, Universités Paris VI and VII, CNRS/IN2P3, Paris, France*
[15]*CEA, Irfu, SPP, Saclay, France*
[16]*IPHC, Université de Strasbourg, CNRS/IN2P3, Strasbourg, France*
[17]*IPNL, Université Lyon 1, CNRS/IN2P3, Villeurbanne, France and Université de Lyon, Lyon, France*
[18]*III. Physikalisches Institut A, RWTH Aachen University, Aachen, Germany*
[19]*Physikalisches Institut, Universität Freiburg, Freiburg, Germany*
[20]*II. Physikalisches Institut, Georg-August-Universität Göttingen, Göttingen, Germany*
[21]*Institut für Physik, Universität Mainz, Mainz, Germany*
[22]*Ludwig-Maximilians-Universität München, München, Germany*
[23]*Fachbereich Physik, Bergische Universität Wuppertal, Wuppertal, Germany*
[24]*Panjab University, Chandigarh, India*
[25]*Delhi University, Delhi, India*
[26]*Tata Institute of Fundamental Research, Mumbai, India*
[27]*University College Dublin, Dublin, Ireland*
[28]*Korea Detector Laboratory, Korea University, Seoul, Korea*
[29]*CINVESTAV, Mexico City, Mexico*
[30]*Nikhef, Science Park, Amsterdam, the Netherlands*
[31]*Radboud University Nijmegen, Nijmegen, the Netherlands*
[32]*Joint Institute for Nuclear Research, Dubna, Russia*
[33]*Institute for Theoretical and Experimental Physics, Moscow, Russia*
[34]*Moscow State University, Moscow, Russia*
[35]*Institute for High Energy Physics, Protvino, Russia*
[36]*Petersburg Nuclear Physics Institute, St. Petersburg, Russia*
[37]*Institució Catalana de Recerca i Estudis Avançats (ICREA) and Institut de Física d'Altes Energies (IFAE), Barcelona, Spain*
[38]*Uppsala University, Uppsala, Sweden*
[39]*Lancaster University, Lancaster LA1 4YB, United Kingdom*
[40]*Imperial College London, London SW7 2AZ, United Kingdom*
[41]*The University of Manchester, Manchester M13 9PL, United Kingdom*
[42]*University of Arizona, Tucson, Arizona 85721, USA*
[43]*University of California Riverside, Riverside, California 92521, USA*
[44]*Florida State University, Tallahassee, Florida 32306, USA*
[45]*Fermi National Accelerator Laboratory, Batavia, Illinois 60510, USA*
[46]*University of Illinois at Chicago, Chicago, Illinois 60607, USA*
[47]*Northern Illinois University, DeKalb, Illinois 60115, USA*
[48]*Northwestern University, Evanston, Illinois 60208, USA*
[49]*Indiana University, Bloomington, Indiana 47405, USA*
[50]*Purdue University Calumet, Hammond, Indiana 46323, USA*
[51]*University of Notre Dame, Notre Dame, Indiana 46556, USA*
[52]*Iowa State University, Ames, Iowa 50011, USA*
[53]*University of Kansas, Lawrence, Kansas 66045, USA*

[54]Kansas State University, Manhattan, Kansas 66506, USA
[55]Louisiana Tech University, Ruston, Louisiana 71272, USA
[56]Boston University, Boston, Massachusetts 02215, USA
[57]Northeastern University, Boston, Massachusetts 02115, USA
[58]University of Michigan, Ann Arbor, Michigan 48109, USA
[59]Michigan State University, East Lansing, Michigan 48824, USA
[60]University of Mississippi, University, Mississippi 38677, USA
[61]University of Nebraska, Lincoln, Nebraska 68588, USA
[62]Rutgers University, Piscataway, New Jersey 08855, USA
[63]Princeton University, Princeton, New Jersey 08544, USA
[64]State University of New York, Buffalo, New York 14260, USA
[65]University of Rochester, Rochester, New York 14627, USA
[66]State University of New York, Stony Brook, New York 11794, USA
[67]Brookhaven National Laboratory, Upton, New York 11973, USA
[68]Langston University, Langston, Oklahoma 73050, USA
[69]University of Oklahoma, Norman, Oklahoma 73019, USA
[70]Oklahoma State University, Stillwater, Oklahoma 74078, USA
[71]Brown University, Providence, Rhode Island 02912, USA
[72]University of Texas, Arlington, Texas 76019, USA
[73]Southern Methodist University, Dallas, Texas 75275, USA
[74]Rice University, Houston, Texas 77005, USA
[75]University of Virginia, Charlottesville, Virginia 22904, USA
[76]University of Washington, Seattle, Washington 98195, USA

(Dated: July 24, 2012)

We present a search for the standard model (SM) Higgs boson produced in association with a Z boson in 9.7 fb^{-1} of $p\bar{p}$ collisions collected with the D0 detector at the Fermilab Tevatron Collider at $\sqrt{s} = 1.96$ TeV. Selected events contain one reconstructed $Z \to e^+e^-$ or $Z \to \mu^+\mu^-$ candidate and at least two jets, including at least one jet identified as likely to contain a b quark. To validate the search procedure, we also measure the cross section for ZZ production in the same final state. It is found to be consistent with its SM prediction. We set upper limits on the ZH production cross section times branching ratio for $H \to b\bar{b}$ at the 95% C.L. for Higgs boson masses $90 \leq M_H \leq 150$ GeV. The observed (expected) limit for $M_H = 125$ GeV is 7.1 (5.1) times the SM cross section.

PACS numbers: 13.85.Ni, 13.85.Qk, 13.85.Rm, 14.80.Bn

In the standard model (SM), the spontaneous breaking of the electroweak gauge symmetry generates masses for the W and Z bosons and produces a residual massive particle, the Higgs boson [1]. Precision electroweak data, including the latest W boson mass measurements from the CDF [2] and D0 [3] Collaborations, and the latest Tevatron combination for the top quark mass [4] constrain the mass of the SM Higgs boson to $M_H < 152$ GeV [5] at the 95% confidence level (C.L.). Direct searches at the CERN e^+e^- Collider (LEP) [6], by the CDF and D0 Collaborations at the Fermilab Tevatron $p\overline{p}$ Collider [7], and by the ATLAS and CMS Collaborations at the CERN Large Hadron Collider (LHC) [8, 9] further restrict the allowed range to $116.6 < M_H < 119.4$ GeV and $122.1 < M_H < 127.0$ GeV. The ATLAS and CMS results indicate excesses above background expectations at $M_H \approx 125$ GeV. With additional data and analysis improvements, the LHC experiments confirm their initial indications and observe a particle with properties consistent with those predicted for the SM Higgs boson [10].

For $M_H \lesssim 135$ GeV, the primary decay is to the $b\bar{b}$ final state [11]. At the Tevatron, the best sensitivity to a SM Higgs boson in this mass range is obtained from the analysis of its production in association with a W or Z boson and its subsequent decay into $b\bar{b}$. Evidence for a signal in this decay mode would complement the LHC findings and provide further indication that the new particle is the SM Higgs boson.

We present a search for $ZH \to \ell^+\ell^- b\bar{b}$ events, where ℓ is either a muon or an electron. The data for this analysis were collected at the Tevatron at $\sqrt{s} = 1.96$ TeV with the D0 detector from April 2002 to September 2011 and correspond to an integrated luminosity of 9.7 fb^{-1} after data quality requirements are imposed, which represents the full Run II data set. To validate the search procedure, we also present a measurement of the ZZ production cross section in the same final states and topologies used for the search. The results presented here supersede our previous search in the $ZH \to \ell^+\ell^- b\bar{b}$ channel [12].

*with visitors from [a]Augustana College, Sioux Falls, SD, USA, [b]The University of Liverpool, Liverpool, UK, [c]UPIITA-IPN, Mexico City, Mexico, [d]DESY, Hamburg, Germany, [e]SLAC, Menlo Park, CA, USA, [f]University College London, London, UK, [g]Centro de Investigacion en Computacion - IPN, Mexico City, Mexico, [h]ECFM, Universidad Autonoma de Sinaloa, Culiacán, Mexico and [i]Universidade Estadual Paulista, São Paulo, Brazil.

Beyond the inclusion of additional data, the most significant updates to this analysis are the use of an improved b-jet identification algorithm, revisions to the kinematic fit, and a new multivariate analysis strategy. A search for $ZH \to \ell^+\ell^- b\bar{b}$ has also been performed by the CDF Collaboration [13].

The D0 detector [14, 15] consists of a central tracking system within a 2 T superconducting solenoidal magnet and surrounded by a preshower detector, three liquid-argon sampling calorimeters, and a muon spectrometer with a 1.8 T iron toroidal magnet. In the intercryostat regions (ICRs) between the central and end calorimeter cryostats, plastic scintillator detectors enhance the calorimeter coverage. The analyzed events were acquired predominantly with triggers that select electron and muon candidates online. However, events satisfying any trigger requirement are considered in this analysis.

The event selection requires a $p\overline{p}$ interaction vertex that has at least three associated tracks. Selected events must contain a $Z \to \ell^+\ell^-$ candidate. The analysis is conducted in four separate channels. The dimuon ($\mu\mu$) and dielectron (ee) channels include events with at least two fully reconstructed muons or electrons. In addition, muon-plus-track ($\mu\mu_{\rm trk}$) and electron-plus-ICR electron ($ee_{\rm ICR}$) channels are designed to recover events in which one of the leptons points to a poorly instrumented region of the detector.

The $\mu\mu$ event selection requires at least two muons identified in the muon system, both matched to central tracks with transverse momenta $p_T > 10$ GeV. At least one muon must have $|\eta| < 1.5$, where η is the pseudorapidity, and $p_T > 15$ GeV. At least one of the muons must be separated from any jet with $p_T > 20$ GeV and $|\eta| < 2.5$ by $\Delta\mathcal{R} = \sqrt{\Delta\eta^2 + \Delta\phi^2} > 0.5$, from other tracks, and from energy deposited in the calorimeter. We also apply isolation requirements based on the ratios of the calorimeter energy and the sum of p_T of tracks near the lepton to the lepton p_T in this analysis.

The $\mu\mu_{\rm trk}$ event selection requires exactly one muon with $|\eta| < 1.5$ and $p_T > 15$ GeV that is isolated both in the tracker and in the calorimeter. In addition, a second isolated track reconstructed in the tracker with $|\eta| < 2$ and $p_T > 20$ GeV must be present. Its distance $\Delta\mathcal{R}$ from the muon and from any jet of $p_T > 15$ GeV and $|\eta| < 2.5$ must be greater than 0.1 and 0.5, respectively. For the $\mu\mu$ and $\mu\mu_{\rm trk}$ channels, the two muon-associated tracks must have opposite charge.

The ee event selection requires at least two electrons with transverse energy $E_T > 15$ GeV that pass selection requirements based on the energy deposition and shower shape in the calorimeter and the preshower detector. Both electrons are required to be isolated in the tracker and the calorimeter. At least one electron must be identified in the region $|\eta| < 1.1$. The electrons in $|\eta| < 1.1$ must match central tracks or a set of hits in the tracker consistent with that of an electron trajectory.

The $ee_{\rm ICR}$ event selection requires exactly one electron in the calorimeter with $E_T > 15$ GeV and a track pointing toward one of the ICRs, $1.1 < |\eta| < 1.5$. The track must be isolated, be matched to a calorimeter energy deposit with $E_T > 10$ GeV and have $p_T > 15$ GeV. For the ee and $ee_{\rm ICR}$ selections, electrons must be separated from all jets by $\Delta\mathcal{R} > 0.5$.

Jets are reconstructed in the calorimeter by using the iterative midpoint cone algorithm [16] with a cone of radius 0.5 in rapidity and azimuthal angle. The jet identification efficiency is $\approx 95\%$ at $p_T = 20$ GeV and reaches 99% at $p_T = 50$ GeV. Jets are denoted as "taggable" if the associated tracks meet criteria that algorithms to identify jets as likely to contain b-quarks operate efficiently. The taggability efficiency is at least 90% for most of the jets in this analysis. We use "inclusive" to denote the event sample selected by requiring the presence of two leptons and use "pretag" for the event sample that meets the additional requirements of having at least two taggable jets with $p_T > 20$ GeV and $|\eta| < 2.5$ and a dilepton invariant mass $70 < m_{\ell\ell} < 110$ GeV [17].

Jets are identified as likely to contain b quarks (b-tagged) if they pass "loose" or "tight" requirements on the output of a multivariate discriminant trained to separate b jets from light jets. This discriminant is an improved version of the neural network b-tagging discriminant described in Ref. [18]. For taggable jets in $|\eta| < 1.1$ and with $p_T \approx 50$ GeV, the b-tagging efficiency for b jets and the misidentification probability of light (uds or gluon) jets are, respectively, 72% and 6.7% for loose b tags, and 47% and 0.4% for tight b tags. Events with at least one tight and one loose b tag are classified as double-tagged (DT). Events not in the DT sample that contain a single tight b tag are classified as single-tagged (ST).

The dominant background process is the production of a Z boson in association with jets, with the Z decaying to dileptons (Z+jets). The light-flavor component (Z+LF) includes jets from only light quarks or gluons. The heavy-flavor component (Z+HF) includes $Z + b\bar{b}$, which has the same final state as the signal, and $Z + c\bar{c}$ production. The remaining backgrounds are from $t\bar{t}$ production; WW, WZ, and ZZ (diboson) production; and multijet (MJ) events with nonprompt muons or with jets misidentified as electrons.

We simulate ZH and diboson production with PYTHIA [19]. In the ZH samples, we consider the contributions to the signal from the $\ell^+\ell^- b\bar{b}$, $\ell^+\ell^- c\bar{c}$, and $\ell^+\ell^-\tau^+\tau^-$ final states. The $\ell^+\ell^- b\overline{b}$ accounts for 99% (97%) of the signal yield in the DT (ST) sample. The Z+jets and $t\bar{t}$ processes are simulated with ALPGEN [20], followed by PYTHIA for parton showering and hadronization [21]. All simulated samples are generated by using the CTEQ6L1 [22] leading-order parton distribution functions. We process all samples by using a detector simulation program based on GEANT3 [23] and the same offline reconstruction algorithms used for data. We overlay events from randomly chosen beam crossings with the same instantaneous luminosity distribution as data on the generated events to model the effects of multiple

$p\bar{p}$ interactions and detector noise.

We take the cross sections and branching ratios for signal from Refs. [11, 24]. For the diboson processes, we use next-to-leading order (NLO) cross sections from the Monte Carlo program MCFM [25]. We scale the $t\bar{t}$ cross section to approximate next-to-NLO [26] and the inclusive Z boson cross section to next-to-NLO [27] and apply additional NLO heavy-flavor corrections to the $Z+b\bar{b}$ and $Z+c\bar{c}$ samples, calculated from MCFM to be 1.52 and 1.67, respectively.

To improve the modeling of the p_T distribution of the Z boson, we reweight simulated Z+jets events to be consistent with the measured p_T spectrum of Z bosons in the data [28]. We correct the energies of simulated jets to reproduce the resolution and energy scale observed in the data [29]. We apply the trigger efficiencies, measured in the data, as event weights to the simulated $\mu\mu$, $\mu\mu_{\rm trk}$ and $ee_{\rm ICR}$ events. In the ee channel, we have verified that the trigger efficiency is consistent with 100% for our selection. We apply scale factors to account for differences in reconstruction efficiency between the data and simulation. Motivated by a comparison with data [30] and the SHERPA generator [31], we reweight the Z+jets events to improve the ALPGEN modeling of the distributions of the η of the two jets.

We estimate the MJ backgrounds from control samples in data obtained by inverting some of the lepton selection requirements, e.g., the lepton isolation requirements in the $\mu\mu$ channel and the shower shape requirements in the ee channel. We adjust the normalizations of the MJ background and all simulated samples by scale factors determined from a simultaneous fit to the $m_{\ell\ell}$ distributions in the 0-jet, 1-jet, and $\geq$ 2-jet samples of each lepton selection. The inclusive sample constrains the lepton trigger and identification efficiencies, while the pretag sample, which includes jet requirements, is used to correct the Z+jets cross section. The total event yields after applying all corrections and normalization factors are shown in Table I. The observed event yields are consistent with the expected background.

To exploit the fully constrained kinematics of the $ZH \to \ell^+\ell^- b\bar{b}$ process, we adjust the energies of the candidate leptons and jets within their experimental resolutions by using a likelihood fit that constrains $m_{\ell\ell}$ to the mass and width of the Z boson and constrains the p_T of the $\ell^+\ell^- b\bar{b}$ system to zero with an expected width determined from ZH Monte Carlo events. This kinematic fit improves the dijet mass resolution by 10%$-$15%, depending on M_H. The dijet mass resolution for $M_H = 125$ GeV is $\approx$ 15 GeV with the kinematic fit [17].

We use a two step multivariate analysis strategy based on random forest (RF, an ensemble classifier that consists of many decision trees) discriminants [32], as implemented in the TMVA software package [33], to improve the separation of signal from background [17]. We choose well modeled kinematic variables that are sensitive to the ZH signal as inputs for the analysis. These include the p_T of the two b-jet candidates and the dijet mass, before and after the jet energies are adjusted by the kinematic fit. In the first step, we train a dedicated RF ($t\bar{t}$ RF) that takes $t\bar{t}$ as the only background and ZH as the signal. This approach takes advantage of the characteristic signature of the $t\bar{t}$ background, for instance, the presence of large missing transverse energy. In the second step, we use the $t\bar{t}$ RF to define two independent regions: a $t\bar{t}$ enriched region ($t\bar{t}$ RF < 0.5) and a $t\bar{t}$ depleted region ($t\bar{t}$ RF ≥ 0.5). The $t\bar{t}$ depleted region contains 94% (93%) of the DT (ST) signal contribution and 55% (82%) of DT (ST) background events. In each region, we train a global RF to separate the ZH signal from all backgrounds. In both steps we consider ST and DT events separately and train the discriminants for each assumed value of M_H in 5 GeV steps from 90 to 150 GeV.

We assess systematic uncertainties resulting from the background normalization for the MJ contribution, typically 10%. The normalization of the Z+jets sample to the pretag data constrains that sample to the statistical uncertainty, <1%, of the pretag data. Because this sample is dominated by the Z+LF background, the normalization of the $t\bar{t}$, diboson, and ZH samples acquires a sensitivity to the inclusive Z cross section, for which we assess a 6% uncertainty [27]. We assign this uncertainty to these samples as a common uncertainty. For Z+HF, a cross section uncertainty of 20% is determined from Ref. [25]. For other backgrounds, the uncertainties are 6%–10% [25, 26]. For the signal, the cross section uncertainty is 6% [24]. Sources of systematic uncertainty affecting the shapes of the final discriminant distributions are the jet energy scale, 1%–3%; jet energy resolution, 2%–4%; jet identification efficiency, $\approx$ 4%; and b-tagging efficiency, 4%–6%. Other sources include trigger efficiency, 4%–6%; parton distribution function uncertainties [34], <1%; data-determined corrections to the model for Z+jets, 3%–4%; modeling of the underlying event, <1%; and from varying the factorization and renormalization scales for the Z+jets simulation, <1%.

The global RF distributions from the four samples (ST and DT in the $t\bar{t}$ depleted and $t\bar{t}$ enriched regions) in each channel along with the corresponding systematic uncertainties are used for the statistical analysis of the data. We set 95% C.L. upper limits on the ZH cross section times branching ratio for $H \to b\bar{b}$ with a modified frequentist (CL$_s$) method that uses the log likelihood ratio of the signal+background (S+B) hypothesis to the background-only (B) hypothesis [35]. To minimize the effect of systematic uncertainties, we maximize the likelihoods of the B and S+B hypotheses by independent fits that allow the sources of systematic uncertainty to vary within their Gaussian priors [36].

To validate the search procedure, we search for ZZ production in the $\ell^+\ell^- b\bar{b}$ and $\ell^+\ell^- c\bar{c}$ final states. We use the same event selection, corrections to our signal and background models, and RF training procedure as for the ZH search [17]. Our search also includes WZ production in the $c\bar{s}\ell^+\ell^-$ final state. We collectively refer to these as VZ production. Using the same modified

TABLE I: Expected and observed event yields for all lepton channels combined after requiring two leptons (inclusive), after also requiring at least two jets (pretag), and after requiring exactly one (ST) or at least two (DT) b-tags. The ZH signal yields are for $M_H = 125$ GeV. The uncertainties quoted on the total background for ST and DT and signal include the statistical and systematic uncertainties.

	Data	Total background	MJ	Z+LF	Z+HF	Diboson	$t\bar{t}$	ZH
Inclusive	1845610	1841683	160746	1630391	46462	2914	1170	17.3 ± 1.1
Pretag	25849	25658	1284	19253	4305	530	285	9.2 ± 0.6
ST	886	824 ± 102	54	60	600	33	77	2.5 ± 0.2
DT	373	366 ± 39	25.7	3.5	219	19	99	2.9 ± 0.2

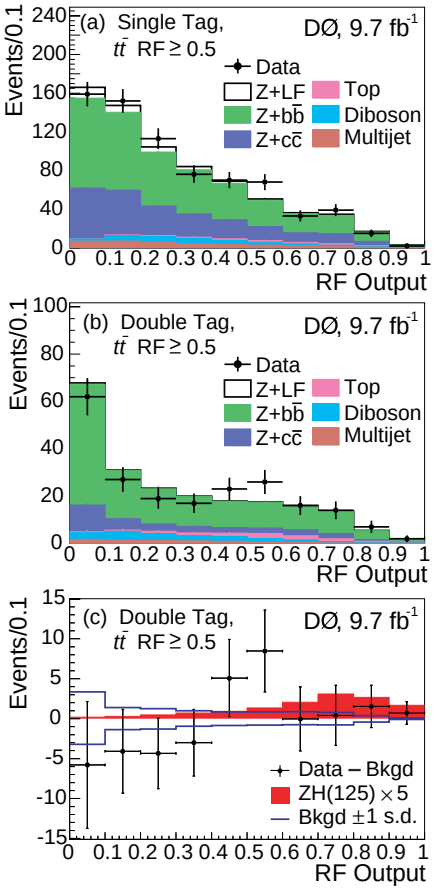

FIG. 1: (color online). Distributions of the global RF discriminant in the $t\bar{t}$ depleted region, assuming $M_H = 125$ GeV, after the fit to the background-only model for data (points with statistical error bars) and background (histograms) for (a) single-tagged events and (b) double-tagged events. (c) Background-subtracted distribution for (b). The signal distribution is shown with the SM cross section scaled by a factor of five. The blue lines indicate the uncertainty from the fit.

frequentist method as for the ZH search and fitting the RF distributions to the S+B hypothesis, we measure a VZ cross section of $0.8 \pm 0.4\,(\text{stat}) \pm 0.4\,(\text{syst})$ times that of the SM prediction with a significance of 1.5 standard deviation (s.d.) and an expected significance of 1.9 s.d. This result is consistent with the recent D0 $ZZ + WZ$ cross section measurement obtained in fully leptonic decay channels [37].

The output of the RF trained to separate signal events with $M_H = 125$ GeV from background is shown in Fig. 1 for ST and DT events separately in the $t\bar{t}$ depleted region, after the background-only fit. Also shown is the background-subtracted RF distribution for DT events in the data. The upper limit on the cross section times branching ratio for $H \to b\bar{b}$, expressed as a ratio to the SM prediction, is presented as a function of M_H in Table II and Fig. 2. At $M_H = 125$ GeV, the observed (expected) limit on this ratio is 7.1 (5.1). The expected limits are $\approx 20\%$ lower than those anticipated from the increase in the data because of the analysis improvements described above.

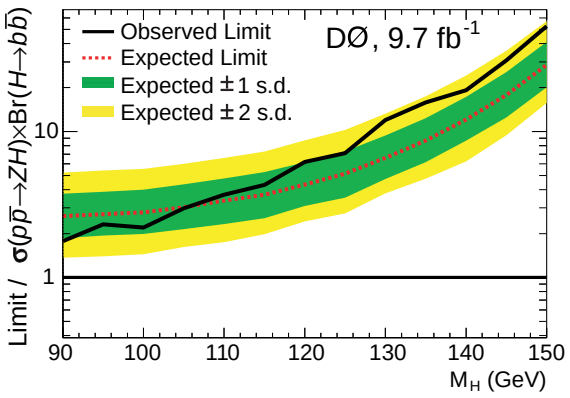

FIG. 2: (color online). Expected and observed 95% C.L. cross section upper limits on the ZH cross section times branching ratio for $H \to b\bar{b}$, expressed as a ratio to the SM prediction.

In summary, we have searched for SM Higgs boson production in association with a Z boson in the final state of two charged leptons (electrons or muons) and two b-quark jets by using a 9.7 fb^{-1} data set of $p\bar{p}$ collisions at $\sqrt{s} = 1.96$ TeV. We also measure the cross section for VZ production in the same final state with the result of $0.8 \pm 0.4\,(\text{stat}) \pm 0.4\,(\text{syst})$ times its SM prediction. We set an upper limit on the ZH production cross section times branching ratio for $H \to b\bar{b}$ as a function of M_H. The observed (expected) limit for $M_H = 125$ GeV is 7.1 (5.1) times the SM cross section.

TABLE II: The expected and observed 95% C.L. upper limits on the ZH production cross section times branching ratio for $ZH \to \ell^+\ell^- b\bar{b}$, expressed as a ratio to the SM prediction.

M_H (GeV)	90	95	100	105	110	115	120	125	130	135	140	145	150
Expected	2.6	2.7	2.8	3.0	3.4	3.7	4.3	5.1	6.6	8.7	12	18	29
Observed	1.8	2.3	2.2	3.0	3.7	4.3	6.2	7.1	12	16	19	31	53

Acknowledgments

We thank the staffs at Fermilab and collaborating institutions, and acknowledge support from the DOE and NSF (USA); CEA and CNRS/IN2P3 (France); FASI, Rosatom and RFBR (Russia); CNPq, FAPERJ, FAPESP and FUNDUNESP (Brazil); DAE and DST (India); Colciencias (Colombia); CONACyT (Mexico); KRF and KOSEF (Korea); CONICET and UBACyT (Argentina); FOM (The Netherlands); STFC and the Royal Society (United Kingdom); MSMT and GACR (Czech Republic); CRC Program and NSERC (Canada); BMBF and DFG (Germany); SFI (Ireland); The Swedish Research Council (Sweden); and CAS and CNSF (China).

[1] F. Englert and R. Brout, Phys. Rev. Lett. **13**, 321 (1964); P.W. Higgs, Phys. Rev. Lett. **13**, 508 (1964); G.S. Guralnik, C.R. Hagen, and T.W.B. Kibble, Phys. Rev. Lett. **13**, 585 (1964).

[2] T. Aaltonen *et al.* (CDF Collaboration), Phys. Rev. Lett. **108**, 151803 (2012).

[3] V.M. Abazov *et al.* (D0 Collaboration), Phys. Rev. Lett. **108**, 151804 (2012).

[4] T. Aaltonen *et al.* [CDF and D0 Collaborations], arXiv:1207.1069 [hep-ex].

[5] LEP Electroweak Working Group http://lepewwg.web.cern.ch/LEPEWWG/.

[6] ALEPH, DELPHI, L3, and OPAL Collaborations, Phys. Lett. B **565**, 61 (2003).

[7] Tevatron New Phenomena and Higgs Working Group, arXiv:1203.3774.

[8] G. Aad *et al.* (ATLAS Collaboration), Phys. Rev. D **86**, 032003 (2012).

[9] S. Chatrchyan *et al.* (CMS Collaboration), Phys. Lett. B **710**, 26 (2012).

[10] G. Aad *et. al.* (ATLAS Collaboration), Phys. Lett. B **716**, 1 (2012); S. Chatrchyan *et. al.* (CMS Collaboration), Phys. Lett. B **716**, 30 (2012).

[11] A. Djouadi, J. Kalinowski, and M. Spira, Comput. Phys. Commun. **108**, 56 (1998); A. Bredenstein, A. Denner, S. Dittmaier, and M.M. Weber, Phys. Rev. D **74** 013004 (2006).

[12] V.M. Abazov *et al.* (D0 Collaboration), Phys. Rev. Lett. **105**, 251801 (2010).

[13] T. Aaltonen *et al.* (CDF Collaboration), Phys. Rev. Lett. **105**, 251802 (2010); Phys. Rev. Lett. **109**, 111803 (2012).

[14] V.M. Abazov *et al.* (D0 Collaboration), Nucl. Instrum. Methods Phys. Res. A **565**, 463 (2006); S. Abachi *et al.* (D0 Collaboration), Nucl. Instrum. Methods Phys. Res. A **338**, 185 (1994).

[15] M. Abolins *et al.*, Nucl. Instrum. Methods Phys. Res. A **584**, 75 (2008); R. Angstadt *et al.*, Nucl. Instrum. Methods Phys. Res. A **622**, 298 (2010); S.N. Ahmed *et al.*, Nucl. Instrum. Methods Phys. Res. A **634**, 8 (2011).

[16] G. C. Blazey *et al.*, arXiv:hep-ex/0005012.

[17] See Appendix.

[18] V.M. Abazov *et al.* (D0 Collaboration), Nucl. Instrum. Methods Phys. Res. A **620**, 490 (2010).

[19] T. Sjöstrand, S. Mrenna, and P. Skands, J. High Energy Phys. **05** (2006) 026; we use version 6.409, D0 Tune A.

[20] M.L. Mangano, F. Piccinini, A.D. Polosa, M. Moretti, and R. Pittau, J. High Energy Phys. **07** (2003) 001. We use version 2.11.

[21] S. Höche *et al.*, arXiv:hep-ph/0602031.

[22] J. Pumplin, D.R.'Stump, J. Huston, H.-L. Lai, P. Nadolsky, and W.-K. Tung, J. High Energy Phys. **07** (2002) 012.

[23] R. Brun and F. Carminati, CERN Program Library Long Writeup W5013 (1993).

[24] J. Baglio and A. Djouadi, J. High Energy Phys. **10** (2010) 064; O. Brein, R.V. Harlander, M. Weisemann, and T. Zirke, Eur. Phys. J. C **72**, 1868 (2012).

[25] J.M. Campbell and R.K. Ellis, Phys. Rev. D **60**, 113006 (1999); **62**, 114012 (2000); **65**, 113007 (2002); J.M. Campbell, R.K. Ellis and C. Williams, http://mcfm.fnal.gov/.

[26] U. Langenfeld, S. Moch, and P. Uwer, Phys. Rev. D **80**, 054009 (2009).

[27] R. Hamberg, W.L. van Neerven, and W.B. Kilgore, Nucl. Phys. **B359**, 343 (1991), **B644**; 403(E) (2002).

[28] V.M. Abazov *et al.* (D0 Collaboration), Phys. Rev. Lett. **100**, 102002 (2008).

[29] V.M. Abazov *et al.* (D0 Collaboration), Phys. Rev. D **85**, 052006 (2012).

[30] V.M. Abazov *et al.* (D0 Collaboration), Phys. Lett. B **669**, 278 (2008).

[31] T. Gleisberg, S. Höche, F.'Krauss, A. Schälicke, S. Schumann, and J.-C. Winter, J. High Energy Phys. **02** (2004) 056; J. Alwall *et al.*, Eur. Phys. J. C **53**, 473 (2008).

[32] L. Breiman, Machine Learning **45**, 5 (2001).

[33] H. Voss *et. al.*, Proc. Sci., (**ACAT2007**) (2007) 040 arXiv:physics/0703039.

[34] D. Stump, J. Huston, J. Pumplin, W.-K. Tung, H.-L. Lai, S. Kuhlmann, and J.F. Owens, J. High Energy Phys. **10** (2003) 046.

[35] T. Junk, Nucl. Instrum. Methods Phys. Res. A **434**, 435 (1999); A. Read. J. Phys. G **28**, 2693 (2002).

[36] W. Fisher, Report No. FERMILAB-TM-2386-E, 2007.

[37] V.M. Abazov *et al.* (D0 Collaboration), Phys. Rev. D **85**,

112005 (2012).

Appendix

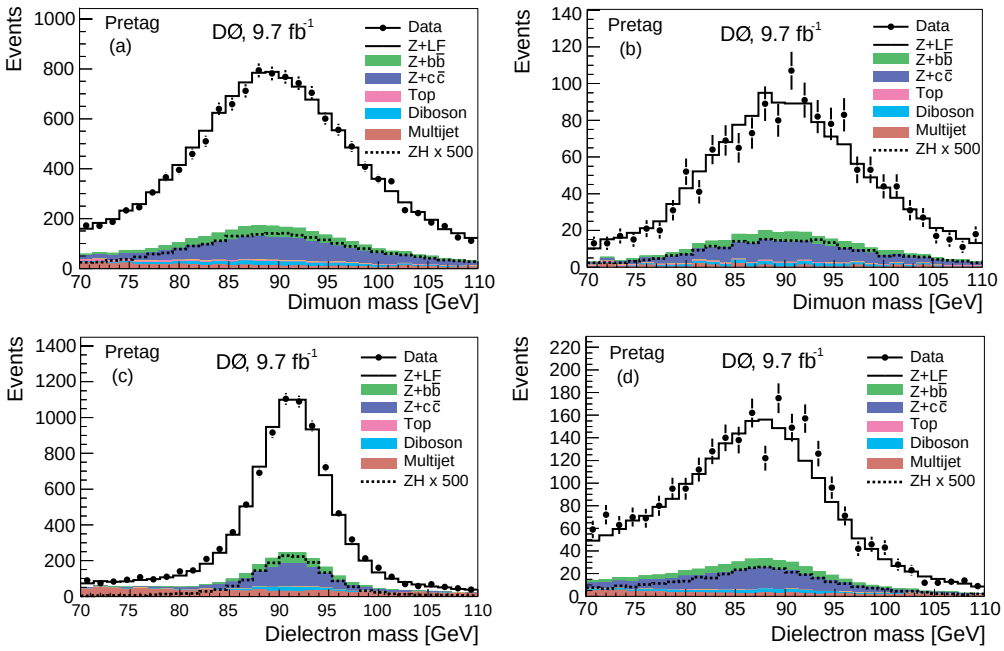

FIG. 3: The dilepton mass spectra in the (a) $\mu\mu$, (b) $\mu\mu_{\rm trk}$, (c) ee and (d) $ee_{\rm ICR}$ channels. Distributions are shown in the pretag control sample, in which all selection requirements except b-tagging are applied. Signal distributions, for $M_H = 125$ GeV, are scaled by a factor of 500.

The dimuon and dielectron mass spectra, after requiring two leptons and at least two jets are shown in Fig. 3. Distributions of the dijet invariant mass spectra before and after adjustment by the kinematic fit, are shown in Fig. 4. A complete list of RF input variables is shown in Table III. Comparisons of the data and MC distributions of the $t\bar{t}$ RF output summed over all lepton channels are shown for $M_H = 125$ GeV in Figure 5. Post-kinematic fit dijet mass distributions for ST and DT in the $t\bar{t}$ depleted region are shown in Fig. 6. Fig. 7 displays the global RF distributions in the $t\bar{t}$ enriched region, after the fit to the background-only hypothesis. Fig. 8 shows the observed LLR as a function of Higgs boson mass. Also shown are the expected (median) LLRs for the background-only and signal+background hypotheses, together with the one and two standard deviation bands about the background-only expectation. Fig. 9 shows the post-fit RF distributions in the $t\bar{t}$ depleted region for the VZ search. Fig. 10 displays the post-fit distribution of the dijet invariant mass from the kinematic fit.

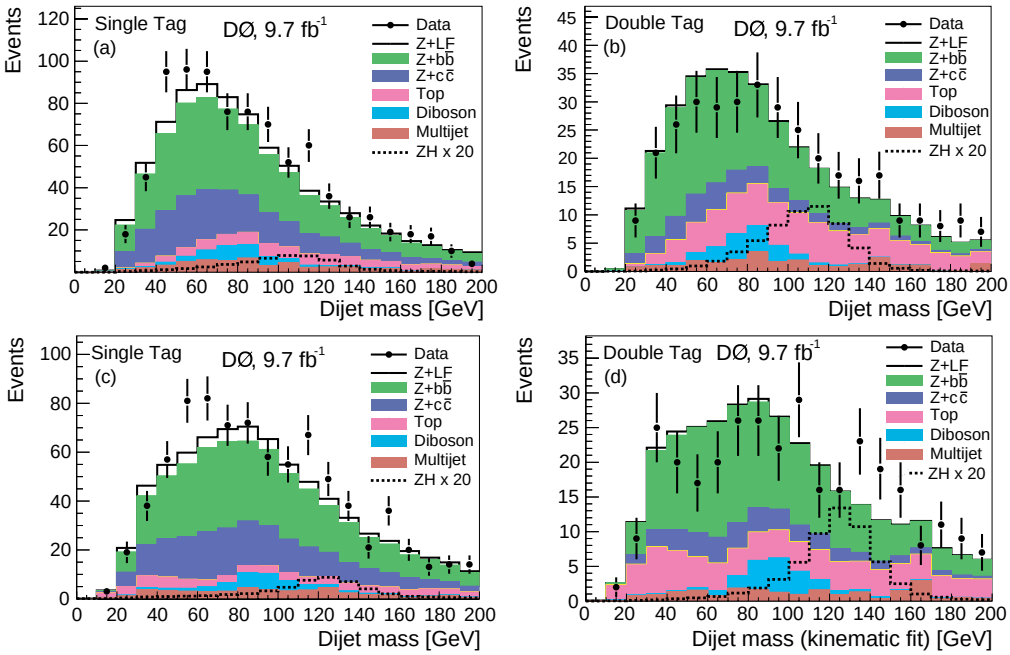

FIG. 4: Dijet invariant mass distributions before the kinematic fit in (a) ST events and (b) DT events; and after the kinematic fit in (c) ST events and (d) DT events, combined for all lepton channels. Signal distributions ($M_H = 125$ GeV) are shown with the SM cross section multiplied by 20.

TABLE III: Variables used for the $t\bar{t}$ and global RF training. The jets that form the Higgs boson candidate are referred to as b_1 and b_2.

variables	definition	tt RF	global RF
m_{bb} ($m_{bb}{}^{fit}$)	invariant mass of the dijet system before (after) the kinematic fit	√	√
p_T^{b1} ($p_T^{b1\,fit}$)	transverse momentum of the first jet before (after) kinematic fit	√	√
p_T^{b2} ($p_T^{b2\,fit}$)	transverse momentum of the second jet before (after) kinematic fit	√	√
p_T^{bb}	transverse momentum of the dijet system before the kinematic fit	√	√
$\Delta\phi(b_1, b_2)$	$\Delta\phi$ between the two jets in the dijet system	–	√
$\Delta\eta(b_1, b_2)$	$\Delta\eta$ between the two jets in the dijet system	–	√
$m(\sum j_i)$	invariant mass of all jets in the event (the multijet mass)	√	√
$p_T(\sum j_i)$	transverse momentum of all jets in the event	√	√
$H_T(\sum j_i)$	scalar sum of the transverse momenta of all jets in the event	√	–
$p_T^{bb}/(\lvert p_T^{b1}\rvert + \lvert p_T^{b2}\rvert)$	ratio of dijet system p_T over the scalar sum of the p_T of the two jets	√	–
$m_{\ell\ell}$	invariant mass of the dilepton system	√	–
p_T^Z	transverse momentum of the dilepton system	√	√
$\Delta\phi(\ell_1, \ell_2)$	$\Delta\phi$ between the two leptons	√	√
colinearity(ℓ_1, ℓ_2)	cosine of the angle between the two leptons (colinearity)	√	√
$\Delta\phi(\ell\ell, bb)$	$\Delta\phi$ between the dilepton and dijet systems	√	√
$\cos\theta^*$	cosine of the angle between the incoming proton and the Z in the zero momentum frame [a]	–	√
$m(\ell\ell bb)$	Invariant mass of dilepton plus dijet system	–	√
$H_T(\ell\ell bb)$	Scalar sum of the transverse momenta of the leptons and jets	–	√
$\not\!\!E_T$	missing transverse energy of the event	√	–
$\not\!\!E_T^{sig}$	the $\not\!\!E_T$ significance [b]	√	√
$-\ln\ L_{fit}$	negative log likelihood from the kinematic fit	√	√
$t\bar{t}$ RF	$t\bar{t}$ RF output	–	√

[a] S. Parke and S. Veseli, Phys. Rev. D **60**, 093003 (1999).
[b] A. Schwartzman, FERMILAB-THESIS-2004-21.

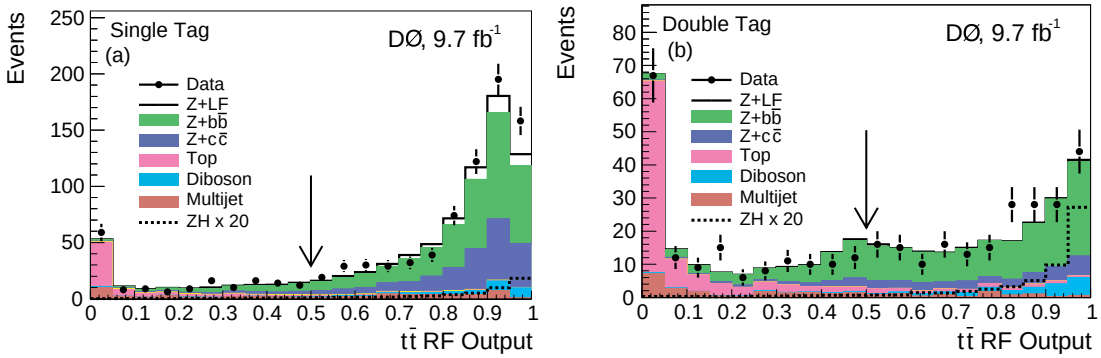

FIG. 5: The $t\bar{t}$ RF output ($M_H = 125$ GeV) for all lepton channels combined (a) ST and (b) DT events. Signal distributions are shown with the SM cross section multiplied by 20. The vertical arrows indicate the $t\bar{t}$ RF selection requirement used to define the $t\bar{t}$ enriched and depleted samples.

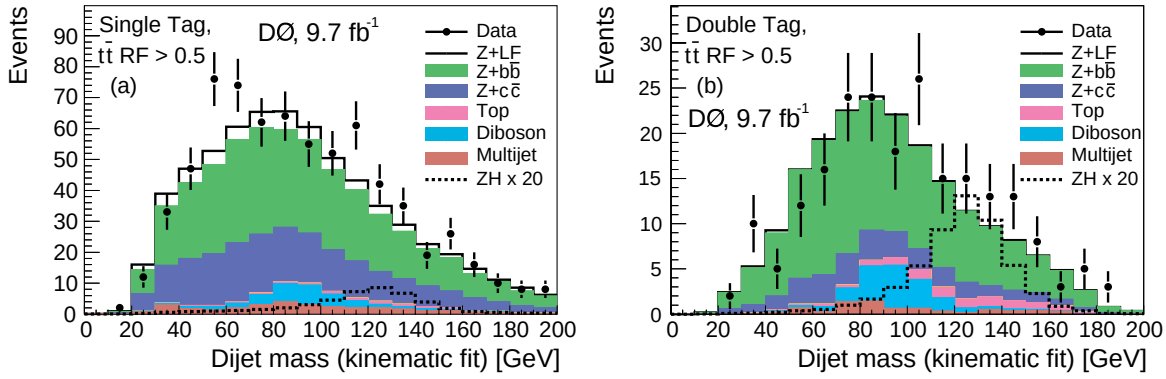

FIG. 6: Post-kinematic fit dijet mass distributions in the $t\bar{t}$ depleted region for all lepton channels combined assuming $M_H = 125$ GeV for (a) ST events and (b) DT events. Signal distributions are shown with the SM cross section multiplied by 20.

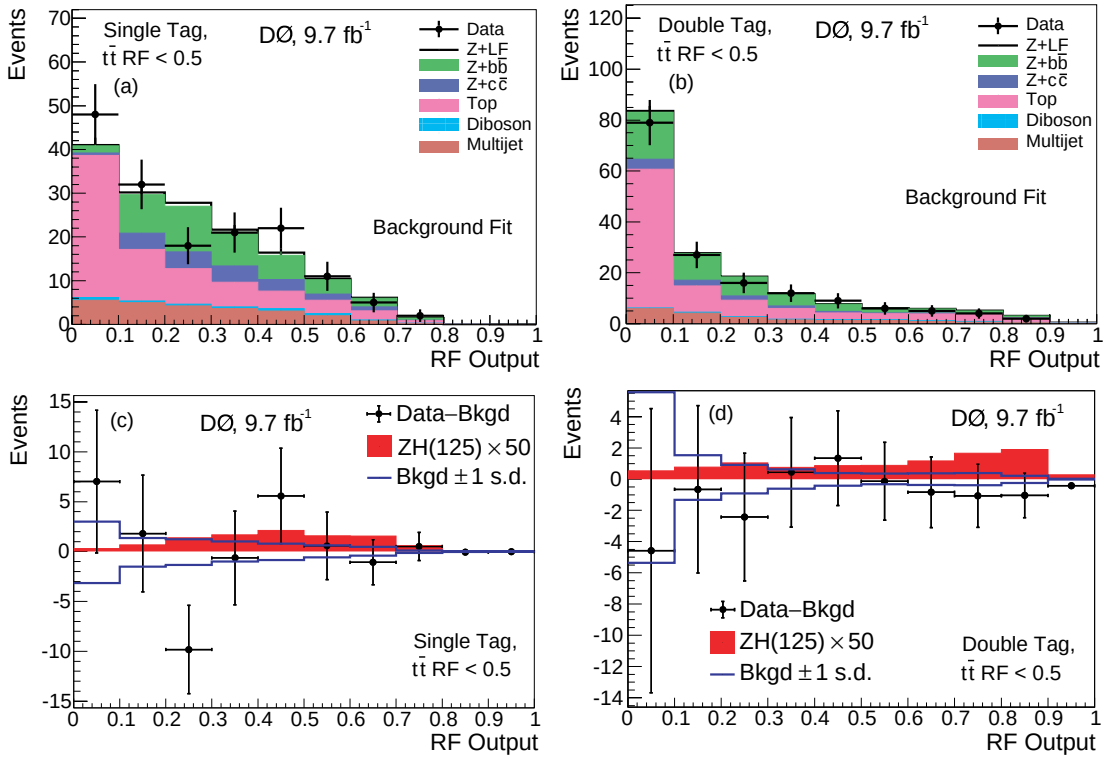

FIG. 7: Post-fit RF output distributions in the $t\bar{t}$ enriched region, assuming $M_H = 125$ GeV, after the fit to the background-only model for (a) ST events and (b) DT events. Background-subtracted distributions for (a) and (b) are shown in (c) and (d), respectively. Signal distributions are shown with the SM cross section scaled to 50 × SM prediction in (c) and (d). The blue lines are the total posterior systematic uncertainty following a fit of the background to the data.

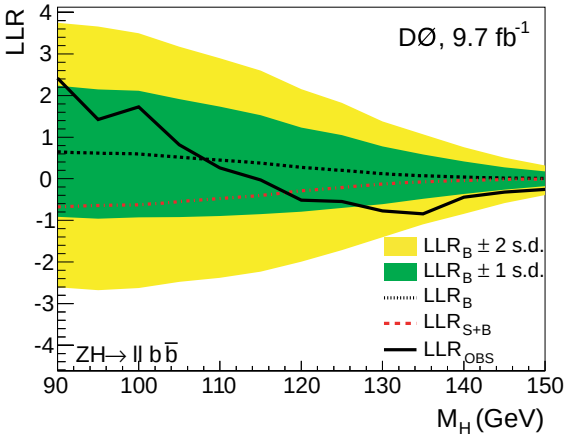

FIG. 8: Observed LLR as a function of Higgs boson mass. Also shown are the expected LLRs for the background-only (B) and signal+background (S+B) hypotheses, together with the one and two standard deviation (s.d.) bands about the background-only expectation.

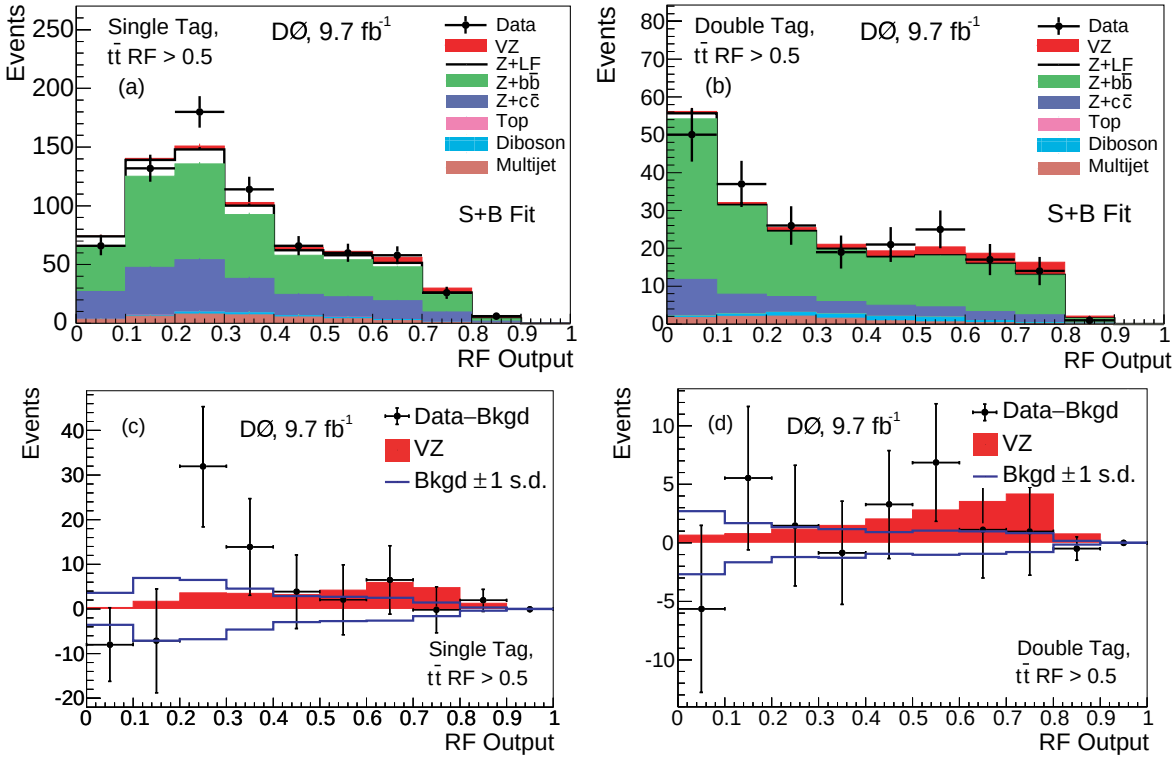

FIG. 9: Post-fit VZ RF output distributions in the $t\bar{t}$ depleted region after the fit to the S+B model for (a) ST events and (b) DT events. Background-subtracted distributions for (a) and (b) are shown in (c) and (d), respectively. Signal distributions are scaled to the measured VZ cross section. The blue lines indicate the uncertainty from the fit.

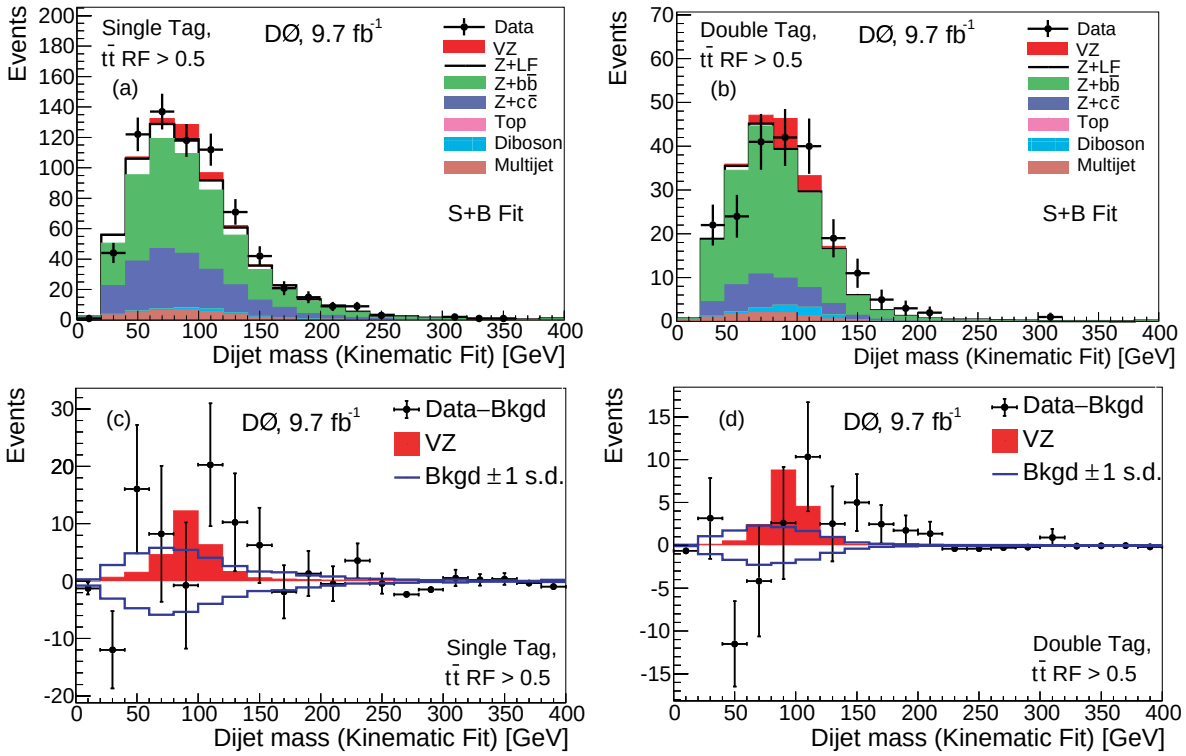

FIG. 10: Post-fit distributions of the dijet invariant mass (from the kinematic fit) in the $t\bar{t}$ depleted region after the fit to the S+B model for (a) ST events and (b) DT events. Background-subtracted distributions for (a) and (b) are shown in (c) and (d), respectively. Signal distributions are scaled to the measured VZ cross section. The blue lines indicate the uncertainty from the fit.